［溶接学会論文集　第 29 巻　第 3 号　p. 53s-57s（2011）］

Numerical Simulation of Fusion Zone Shape of Lotus-type Porous Iron by Laser Welding*

by Takuya Tsumura**, Hideo Nakajima*** and Kazuhiro Nakata**

The effect of direction of unidirectional pores on the fusion zone shape, which produced by laser welding, of lotus-type porous iron was investigated through the numerical simulation of temperature distribution. Three-dimensional heat-transfer analyses, which take into account the thermal properties of the lotus-type porous iron depending on the direction and volume fraction of unidirectional pores, were performed by the ABAQUS FE code with user-defined subroutines. These results indicated that the lotus-type porous iron has little anisotropy of melting property. The calculated shape of weld fusion zone is in good agreement with the cross-sectional view obtained by experiments. In order to clarify the reason of these results, anisotropy of thermal diffusivity in the lotus-type porous copper, magnesium, and iron used and anisotropy of laser energy absorption coefficient for these metals were estimated. As a result, the lotus-type porous iron used has a little difference of thermal diffusivity and laser energy absorption coefficient due to its low thermal conductivity, low porosity, large average pore diameters, and high laser absorption coefficient of base metal.

Key Words: Lotus-type Porous Iron, Laser Welding, Anisotropy, Thermal Diffusivity, Laser Absorption Coefficient

1. Introduction

Lotus- and Gasar- type porous metals had been developed by Boiko[1] and Nakajima et al[2]. These are fabricated by unidirectional solidification under a pressurized gas atmosphere; the pores are aligned parallel to the solidification direction[3]. These were expected as innovative engineering materials because the directional pores yield various unique physical properties such as sound absorption, thermal conductivity, and electrical conductivity[3]. Therefore, laser weldabilities of the lotus-type porous copper[4], iron[5] and magnesium[6] were investigated, and the effect of pore direction on fusion zone shape of the lotus-type porous magnesium[6-9] and copper[8, 9] by using three-dimensional FEM analyses of temperature distribution during laser welding were demonstrated. These reports have pointed out that relation between direction of the pores and the irradiated direction of laser beam appreciably influenced weld formation for the lotus-type porous copper and magnesium; however, the relation had little effect on the weld formation for the lotus-type porous iron.

In the present paper, we performed three-dimensional heat-transfer analysis of temperature distribution during laser welding for the lotus-type porous iron, and compared the fusion zone shape with those cross sections obtained by experiments[5]. We also estimated the anisotropy of thermal diffusivity in the lotus-type porous copper, magnesium, and iron used and the anisotropy of laser energy absorption coefficient for these metals in order to clarify the reason of these results.

*Received: 2008.11.18
**Member, Joining and Welding Research Institute, Osaka University
*** The Institute of Scientific and Industrial Research, Osaka University

2. Experimental procedure and results

Table 1 shows the fabricating conditions and properties of the lotus-type porous metals used. These are the lotus copper[2-4, 10, 11], the lotus magnesium[3, 6, 12-14], and the lotus iron[5, 15]. These metals exhibit different thermal conductivity parallel and normal to the directional pores[6-9, 11]. In order to demonstrate the effect of this characteristic on the welding phenomena, three different combinations of relationships -pore direction, applied heat source direction, and welding direction- were considered as shown in Fig. 1. Here, the first symbol of ⊥ and // in brackets of the combination names indicates the relationship between the pore direction and the applied heat source direction, and the second one indicates the relationship between the pore direction and the welding direction.

Laser welding was conducted using an Nd:YAG laser unit. Laser beam with the wavelength of 1064 nm was irradiated on the lotus iron surface with spot diameter of 1.0 mm and laser power of 1.0 kW at irradiate angle of 32° as shown in Table 1. Argon with a flow rate of 25 $l \cdot \mathrm{min}^{-1}$ was used during welding as the shielding gas. Cross sections of the welded samples were

Table 1 Fabricating conditions and properties of investigated lotus-type porous metals, and laser irradiate angle for laser welding.

	Fabricating conditions		Porosity (%)	Average pore diameters (μm)	Plate thickness (mm)	Irradiate angle (°)
	Fabrication methods	Partial gas-perssure (MPa)				
Lotus copper	Mold casting	H_2:0.25, Ar:0.15	30	100	3	10
Lotus magnesium	Mold casting	H_2:0.9	35	150	1.8	10
Lotus iron	Continuous zone melting	N_2: 2.5	17	370	2	32

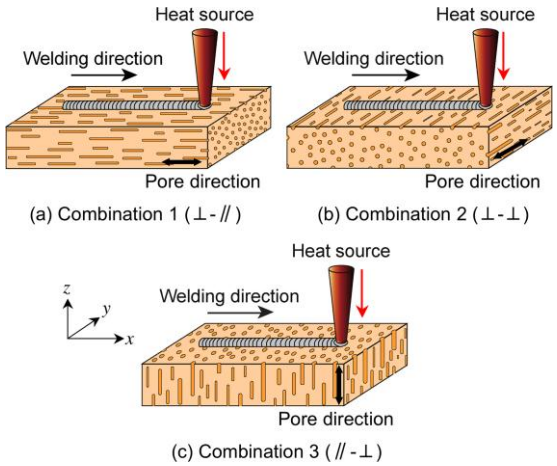

Fig. 1 Schematic views of the lotus-type porous metals showing three combinations of pore direction, applied heat source direction, and welding direction.

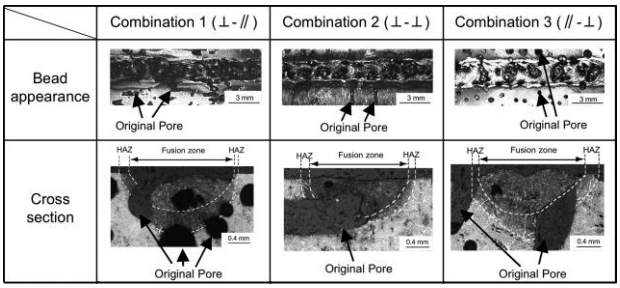

Fig. 2 Bead appearance and cross section of the lotus iron welds; laser power of 1.0 kW, laser spot diameter of 1.0 mm, and welding speed of 1 m·min^{-1} [5].

observed with a digital microscopy.

Figure 2 shows bead appearance and cross section of the lotus iron welds[5]. There is a little difference in the fusion zone shape and penetration depth of the weld bead at the same welding condition among three combinations of direction.

3. Numerical simulation and results

Three-dimensional FEM calculation of temperature distribution of the lotus iron was performed using ABAQUS with user-defined subroutines. The detailed descriptions are given in our previous papers[6-9]. The lotus iron is modeled as an equivalent orthotropic material; Equivalent density $\rho_{eq}(T)$, equivalent specific heat $C_{p\,eq}(T)$, and equivalent thermal conductivity parallel and normal to the directional pores, $k_{eq}^{//}(T)$ and $k_{eq}^{\perp}(T)$, with temperature dependencies are described as the following equations[6-9].

$$\rho_{eq}(T)=(1-\varepsilon)\rho_n(T),\quad C_{p\,eq}(T)=C_{p\,n}(T),$$
$$k_{eq}^{//}(T)=(1-\varepsilon)k_n(T),\quad k_{eq}^{\perp}(T)=(1-\varepsilon)\cdot(1+\varepsilon)^{-1}\cdot k_n(T) \qquad (1)$$

where ε is the pore volume content ratio and is assumed to be temperature independence. The properties of $\rho_n(T)$, $C_{p\,n}(T)$, and $k_n(T)$ with temperature dependency of non-porous iron (AISI 1006) were obtained from the paper[16].

Heat input in the specimen and heat conduction on the specimen surface also considered during laser welding. More detailed descriptions are also given in our previous papers[6-9]. The specimen size, welding speed, and spot diameter were assumed to be 20 mm (x) × 10 mm (y) × 2 mm (z), 1 m·min^{-1}, and 1.0 mm, respectively. Here, the x-y-z coordinate systems defined as shown in Fig. 1 is used. The thermal conductivity $k_{eq}^{//}(T)$ is used at the x direction for the combination 1 $(\perp-//)$, at the y direction for the combination 2 $(\perp-\perp)$, at the z direction for the combination 3 $(//-\perp)$, respectively. The initial temperature of the specimen is 298 K. The ambient temperature was assumed to be constant at 298 K. The analysis region of y>0 is due to the space symmetry because the welding direction is along the x-axis as shown in Fig. 1. Fusion shape of the weld metal is estimated by the cross section of maximum temperature exceeded the melting point (1803 K) at half of the x direction.

Figure 3 shows maximum temperature distributions of the lotus iron. The absorbed laser power shown in Fig.3 (a) is assumed to be 0.522 kW that the most similar results in the combination 2 $(\perp-\perp)$ between the experimental fusion depth as shown in Fig. 2 and the calculated ones. Fusion zone shape has very little difference, and the calculated shapes and the experimental ones were similar. Figure 3 (b) demonstrates the case that the absorbed laser power is 1.5 times larger than that of Fig.3 (a). Fusion zone shape has a little difference among the three different combinations.

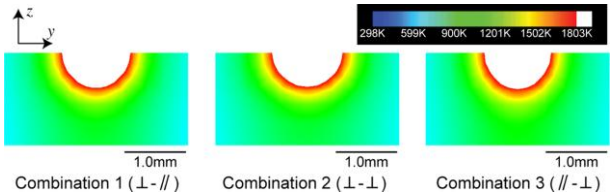

(a) Absorbed laser power of 0.522 kW

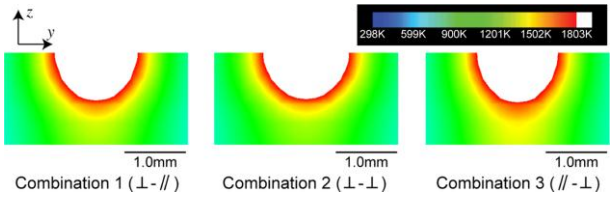

(b) Absorbed laser power of 0.783 kW

Fig. 3 Maximum temperature distributions of the lotus iron in the cross section at half of the welding (x) direction; laser spot diameter of 1.0 mm, and welding speed of 1 m·min^{-1}.

4. Discussions

The relation between direction of the pores and the irradiated direction of laser beam remarkably influenced weld formation for the lotus copper and the lotus magnesium[6-9]; however, the relation effects a little change in the weld formation for the lotus iron as mentioned above. In order to clarify the reason of these results, anisotropy of thermal diffusivity in the lotus-type porous metals and anisotropy of laser energy absorption coefficient for these metals caused by multiple laser reflections on the wall of pores were estimated as follows.

In order to describe the thermal characteristics of a material, the thermal diffusivity α is used in general[17]. This is defined as following equation.

$$\alpha = k \cdot \left(\rho \cdot C_p\right)^{-1} \tag{2}$$

Equivalent thermal diffusivity parallel and normal to the directional pores, $\alpha_{eq}^{//}(T)$ and, $\alpha_{eq}^{\perp}(T)$ are obtained from Eqs. (1) and Eq. (2).

$$\begin{aligned} \alpha_{eq}^{//}(T) &= \frac{k_{eq}^{//}(T)}{\rho_{eq}(T)\cdot C_{p\,eq}(T)} = \alpha_n(T), \\ \alpha_{eq}^{\perp}(T) &= \frac{k_{eq}^{\perp}(T)}{\rho_{eq}(T)\cdot C_{p\,eq}(T)} = (1+\varepsilon)^{-1}\,\alpha_n(T) \end{aligned} \tag{3}$$

Then the ratio of equivalent thermal diffusivity is :

$$\alpha_{eq}^{\perp}(T) / \alpha_{eq}^{//}(T) = (1+\varepsilon)^{-1}. \tag{4}$$

The ratio in Eq. (4) means the degree of anisotropy for the lotus-type porous metals. This is also temperature independence.

Table 2 shows the equivalent thermal diffusivity in Eqs. (3) and its ratio in Eq. (4) of the lotus-type porous metals used at room temperature. These values are estimated from the thermal properties of base metals at room temperature taken from the handbook[18] and the porosity (pore volume content ratio) ε shown in Table 1. The thermal properties of base metals are also shown in Table 2. A comparison of the lotus copper and magnesium case shows that the equivalent thermal diffusivity for the lotus iron is low, the difference between $\alpha_{eq}^{\perp}(T)$ and $\alpha_{eq}^{//}(T)$ is very small, and the ratio is higher than that of the lotus copper and magnesium. Therefore, it can be concluded that due to a combination of low thermal conductivity and low porosity, the anisotropic feature in the lotus iron used is much smaller than that in the lotus copper and magnesium.

Anisotropy of the laser absorption coefficient caused by multiple laser reflections on the wall of pores is also evaluated. As shown in Fig.4, equivalent heat input normal and parallel to the directional pores, $Q_{in}^{\perp}$ and $Q_{in}^{//}$, are described as following equations.

$$\begin{aligned} Q_{in}^{\perp} &= \beta^{\perp} Q = \beta Q, \\ Q_{in}^{//} &= \beta^{//} Q = [(1\text{-}\varepsilon)\beta + (1\text{-}(1\text{-}\beta)^n)\varepsilon]Q \end{aligned} \tag{5}$$

where $\beta^{\perp}$ is the laser absorption coefficient of the lotus-type porous metals for the combination 1 $(\perp - //)$ and combination 2 $(\perp - \perp)$ cases, and it is assumed to be the same of the laser absorption coefficient β on the surface of the base material. $\beta^{//}$ is also the laser absorption coefficient for the

Table 2 Estimated equivalent thermal diffusivity of lotus-type porous metals used at room temperature.

	Thermal properties of base metals (taken form the handbook[18])			Equivalent thermal diffusivity of lotus-type porous metals used		
	ρ_n (Kg m^{-3})	$C_{p\,n}$ (J Kg^{-1} K^{-1})	k_n (W m^{-1} K^{-1})	$\alpha^{\perp}_{eq}$ (×10^{-5} m^2 s^{-1})	$\alpha^{//}_{eq}$ (×10^{-5} m^2 s^{-1})	$\alpha^{\perp}_{eq}/\alpha^{//}_{eq}$
Lotus copper	8880	386	398	8.93	11.61	0.740
Lotus magnesium	1737	1020	156	6.52	8.80	0.769
Lotus iron	7850	465	43	1.01	1.18	0.854

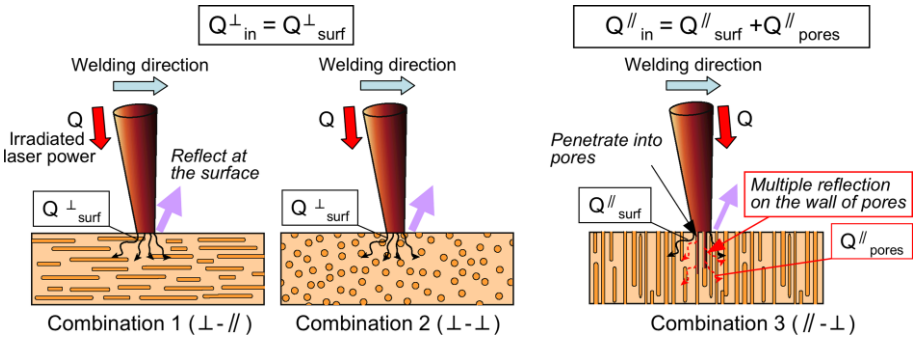

Fig. 4 Schematic illustration of the anisotropy of the equivalent heat input caused by the different combinations of pore direction, irradiated laser direction, and welding direction.

combination 3 $(//-\perp)$ case. In the coefficent $\beta^{//}$, first term indicates the coefficient absorbed only on the top surface, and second term means the increase caused by the multiple laser reflections on the wall of pores.

Figure 5 shows the schematic illustration of multiple reflections of laser beam on the wall of a pore. For this simplified situation, number of multiple reflections n is described by the following equation.

$$n = \mathrm{int}\left(\frac{t}{x}\right) = \mathrm{int}\left(\frac{t\cdot\tan\theta}{d}\right), \quad (6)$$

where t is plate thickness, θ is laser irradiated angle, d is average pore diameters, respectively. Eq. (6) is able to apply directly for the evaluation because almost all of the pores in the investigated lotus-type porous metals pierced through the plate in thickness.

Table 3 shows the number of multiple reflections estimated from Eq. (6), the plate thickness, the laser irradiated angle, and the average pore diameters shown in Table 1. The laser absorption coefficient $\beta^{\perp}$ and $\beta^{//}$ determined from Eqs. (5), and that of base metals β at room temperature, which is taken from the handbook[19], are also shown in Table 3. There is very little difference between $\beta^{\perp}$ and $\beta^{//}$ for the lotus iron. Therefore, it can be concluded that due to a combination of large average pore diameters, low porosity, and high laser absorption coefficient of base metal, the anisotropy of the laser energy absorption coefficient in the lotus iron used is smaller than that in the lotus copper and magnesium.

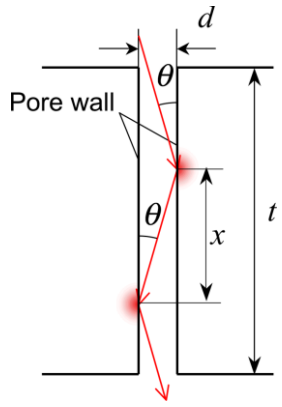

Fig. 5 Schematic illustration of multiple reflections of laser beam on the wall of a pore.

Table 3 Evaluated number of multiple reflections and laser absorption coefficient of the lotus-type porous metals used.

	Number of multiple reflections	Laser absorption coefficient *of* base metals* and lotus metals		
		β	$\beta^{\perp}$	$\beta^{//}$
Lotus copper	5	0.03	0.03	0.063
Lotus magnesium	2	0.26	0.26	0.327
Lotus iron	3	0.41	0.41	0.475

* Wavelength:1000nm at R.T.[19]

5. Conclusions

Three-dimensional heat transfer analysis of temperature distribution during laser welding for the lotus-type porous iron was performed, and the fusion zone shape obtained from the numerical results was compared with those cross sections obtained by experiments. The anisotropy of thermal diffusivity in the lotus-type porous metals used and the anisotropy of the laser energy absorption coefficient were also estimated in order to clarify the reason of the results. The conclusions of this study are summarized as follows.

(1) Fusion zone shape of the weld bead has little difference for three combinations of directions. Calculated shapes and the experimental ones were similar.

(2) The difference between the equivalent thermal diffusivity parallel and normal to the directional pores is small for the lotus iron, due to a combination of low thermal conductivity and low porosity.

(3) The little difference of laser absorption coefficient between $\beta^{\perp}$ and $\beta^{//}$ for the lotus iron, due to a combination of large average pore diameters, low porosity, and high laser absorption coefficient of base metal.

Acknowledgements

This research was supported as part of the entrusted project “development of lightweight high stiffness structural materials and evaluation technology” for the “advanced machining system development project” in the fiscal year 2005 consigned by NEDO. The authors gratefully appreciate this support.

Reference

1) L.V. Boiko: USE OF HYDROGEN FOR THE PRODUCTION OF MATERIALS WITH REGULATED POROSITY, Mater. Sci., 36-4 (2000), 506-512.

2) H. Nakajima, S.K. Hyun, K. Ohashi, K. Ota and K.Murakami: Fabrication of porous copper by unidirectional solidification under hydrogen and its properties, Colloids and Surfaces A, 179 (2001), 209-214.

3) H. Nakajima: Fabrication, properties and application of porous metals with directional pores, Prog. Mater. Sci., 52-7 (2007), 1091-1173.

4) T. Murakami, K. Nakata, T. Ikeda, H. Nakajima and M. Ushio: Weld fusion property of lotus-type porous copper by laser beam irradiation, Mater. Sci. Eng. A, 357 (2003), 134-140.

5) H. Yanagino, T. Tsumura, H. Nakajima, S.K. Hyun and K. Nakata:

Laser welding of Lotus-Type Porous Iron, Mater. Trans., 47-9 (2006), 2254-2258.

6) T. Murakami, T. Tsumura, T. Ikeda, H. Nakajima and K. Nakata: Anisotropic fusion profile and joint strength of lotus-type porous magnesium by laser welding, Mater. Sci. Eng. A, 456 (2007), 278-285.

7) T. Tsumura, T. Murakami, S.K. Hyun, H. Nakajima and K. Nakata: Analysis of Laser Fusion Zone of Lotus-type Porous Metals by 3-dimensional FEM, Mater. Sci. Forum, 502 (2005), 499-504.

8) T. Tsumura, T. Murakami, H. Nakajima and K. Nakata: Numerical Simulation of Laser Fusion Zone Profile of Lotus-Type Porous Metals, Mater. Trans., 47-9 (2006), 2248-2253.

9) T. Tsumura, F. Ye, T. Murakami, H. Nakajima and K. Nakata: Prediction of Laser Fusion Zone Profile of Lotus-type Porous Metals by 3D Heat Transfer Analysis, Soild State Phenomena, 127 (2007), 307-312.

10) S.K. Hyun and H. Nakajima: Anisotropic compressive properties of porous copper produced by unidirectional solidification, Mater. Sci. Eng. A, 340 (2003), 258-264.

11) T. Ogushi, H. Chiba, H. Nakajima and T. Ikeda: Measurement and analysis of effective thermal conductivities of lotus-type porous copper, J. Appl. Phys., 95-10 (2004), 5843-5847.

12) T. Ikeda and H. Nakajima: Fabrication and Mechanical Property of Lotus-type Porous Magnesium, J. Jpn. Foundry Eng. Soc. 74-12 (2002), 812-816 (in Japanese).

13) T. Ikeda, H. Hoshiyama and H. Nakajima: Fabrication and mechanical properties of lotus-type porous magnesium and its alloys, J. Jpn. Inst. Light Met. 54-9 (2004), 388-393 (in Japanese).

14) Z.K. Xie, T. Ikeda, Y. Okuda and H. Nakajima: Characteristics of Sound Absorption in Lotus-Type Porous Magnesium, Jpn. J. Appl. Phys. 43-10 (2004), 7315-7319.

15) M. Tane, T. Ichitsubo, H. Nakajima, S.K. Hyun and M. Hirano: Elastic properties of lotus-type porous iron: acoustic measurement and extended effective-mean-field theory, Acta Mater. 52 (2004), 5195-5201.

16) M.R. Frewin and D.A. Scott: Finite Element Model of Pulsed Laser Welding, Welding Research Supplement, (1999), pp. 15s-22s.

17) A. L. Philips Ed.: Welding Handbook, Sixth ed., Section One, Fundamentals of Welding (1968), p. 2.4.

18) Japan Society of Thermophysical Properties Ed.: Thermophysical Properties Handbook, Yokendo LTD, Tokyo, (1990), p. 23 (in Japanese).

19) E.A. Brandes: Smithells Metal Reference Book, 6th ed., Butterworths, London, (1983), p. 17-7.